Requirement for RORγ in Thymocyte Survival and Lymphoid Organ Development

Zuoming Sun,[1] Derya Unutmaz,[1] Yong-Rui Zou,[1] Mary Jean Sunshine,[1,2] Alessandra Pierani,[3] Susan Brenner-Morton,[3,4] Reina E. Mebius,[5] Dan R. Littman[1,2]*

Most developing thymocytes undergo apoptosis because they cannot interact productively with molecules encoded by the major histocompatibility complex. Here, we show that mice lacking the orphan nuclear hormone receptor RORγ lose thymic expression of the anti-apoptotic factor Bcl-xL. RORγ thus regulates the survival of $CD4^+8^+$ thymocytes and may control the temporal window during which thymocytes can undergo positive selection. RORγ was also required for development of lymph nodes and Peyer's patches, but not splenic follicles. In its absence, there was loss of a population of $CD3^-CD4^+CD45^+$ cells that normally express RORγ and that are likely early progenitors of lymphoid organs. Hence, RORγ has critical functions in T cell repertoire selection and lymphoid organogenesis.

During selection of a T cell repertoire within the thymus, $CD4^+CD8^+$ (double positive, DP) thymocytes with T cell antigen receptors (TCRs) that recognize complexes of host major histocompatibility complex (MHC) proteins and peptides survive and are exported to the periphery (*1*). Cells undergo apoptosis if they have strongly self-reactive TCRs or fail to interact productively with MHC/peptide complexes (*2*). The latter process, termed "death by neglect," accounts for more than 90% of thymocyte death and weeds out useless cells from the developing thymus. It has been proposed that activation of the glucocorticoid receptor by endogenous corticosteroids regulates apoptosis of DP thymocytes (*3*), but other members of the nuclear receptor superfamily have also been implicated in thymocyte selection (*4*). We studied the role of a retinoic acid receptor-related orphan receptor, TOR or RORγ, which is expressed in thymus and skeletal muscle but not in mature T cells (*5, 6*). A thymus-specific isoform of RORγ, RORγt, which shares the DNA and ligand-binding domains with RORγ but differs in the NH_2-terminus, protects hybridomas from TCR-induced apoptosis by inhibiting expression of Fas ligand and interleukin-2 (IL-2) (*7*), probably by its ability to block the function of NFAT (nuclear factor of activated T cells) transcription factors (*8*).

The ability of RORγ to inhibit FasL and cytokine gene expression suggested that this nuclear receptor may regulate apoptosis during thymocyte development. We therefore generated RORγ-deficient mice by gene targeting (*9*). *RORγ*$^{-/-}$ mice were born healthy in a Mendelian distribution, had no discernible physical defect, and were fertile. RORγ mRNA and protein were undetectable in the thymus of homozygous mutant mice, confirming the complete inactivation of the *RORγ* gene and loss of expression of RORγ and the thymus-specific RORγt isoform (*10*).

The thymi of *RORγ*$^{-/-}$ animals appeared normal in size, but total cell numbers recovered were ~30 to 50% of wild-type levels. Flow cytometric analysis showed a reduction in DP thymocyte number (Fig. 1A). Thymocytes also displayed higher forward scatter (FSC), indicative of larger cell size, than did wild-type cells (Fig. 1B), and most FSC^{high} cells were confined to the DP compartment (*11*). The amount of CD4 and TCR expressed was reduced in DP cells from *RORγ*$^{-/-}$ mice (Fig. 1, C and D). However, $CD4^+CD8^-$ single-positive (CD4 SP) cells, although reduced in number, expressed normal amounts of both CD4 and TCR, suggesting that they had undergone positive selection (Fig. 1, C and E). Earlier developmental stages appeared normal in *RORγ*$^{-/-}$ mice, as assessed by the number of double-negative ($CD4^-CD8^-$) thymocytes and by CD44 and CD25 expression (*11*).

To determine whether reduced DP thymocyte cellularity was caused by increased cell death, we performed an ex vivo apoptosis

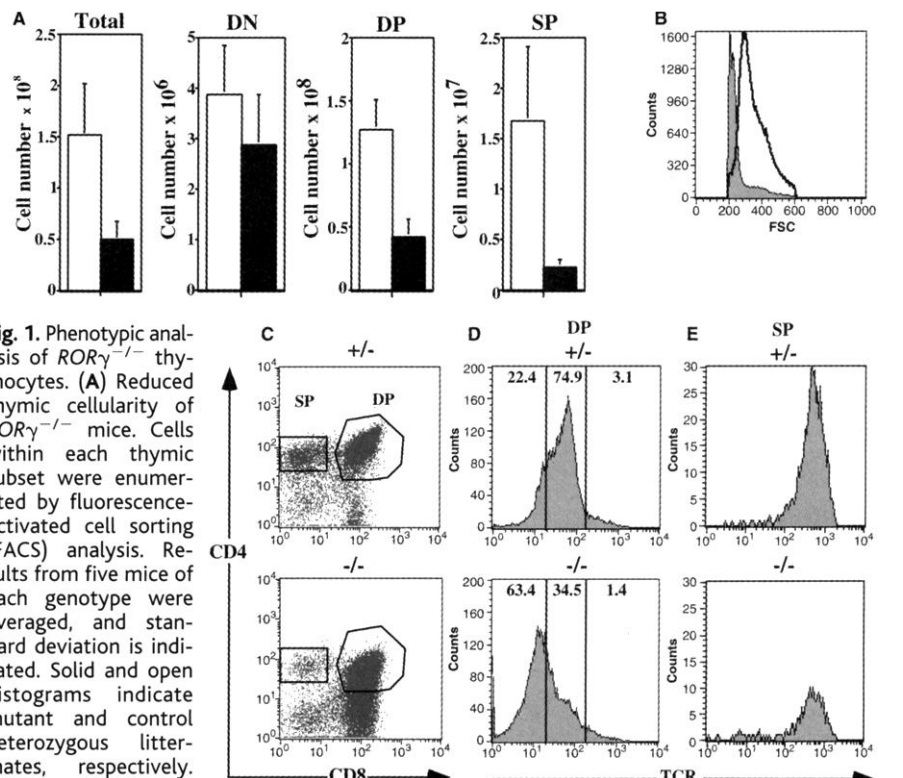

Fig. 1. Phenotypic analysis of *RORγ*$^{-/-}$ thymocytes. (**A**) Reduced thymic cellularity of *RORγ*$^{-/-}$ mice. Cells within each thymic subset were enumerated by fluorescence-activated cell sorting (FACS) analysis. Results from five mice of each genotype were averaged, and standard deviation is indicated. Solid and open histograms indicate mutant and control heterozygous littermates, respectively. (**B**) FSC profile of thymocytes from heterozygous (gray trace) and homozygous mutant (open trace) mice. (**C**) Surface expression of CD4 versus CD8 on thymocytes. (**D**) TCR levels in DP thymocytes from wild-type and mutant mice [as gated in (C)]. Percentages of DP thymocytes expressing low, intermediate, and high levels of TCR are indicated. (**E**) TCR levels in CD4 single-positive thymocytes, as gated in (C).

[1]Molecular Pathogenesis Program, Skirball Institute of Biomolecular Medicine and [2]Howard Hughes Medical Institute, New York University School of Medicine, New York, NY 10016, USA. [3]Department of Biochemistry and Molecular Biophysics and [4]Howard Hughes Medical Institute, Columbia University, New York, NY 10032, USA. [5]Faculty of Medicine, Department of Cell Biology and Immunology, Vrije Universiteit, 1081 BT Amsterdam, Netherlands.

*To whom correspondence should be addressed. E-mail: littman@saturn.med.nyu.edu

time course analysis (Fig. 2A). About 80% of the *RORγ*$^{-/-}$ thymocytes underwent spontaneous apoptosis after 5 hours, compared to only 20% of thymocytes from heterozygous littermates, and the accelerated apoptosis was confined to DP cells (*11*). TUNEL analysis (*2, 12*) showed localization of apoptotic *RORγ*$^{-/-}$ cells within cortical regions, where the DP thymocytes reside (Fig. 2B). Multiprobe ribonuclease (RNase) protection assays of *RORγ*$^{-/-}$ thymocytes showed that the amount of Bcl-xL mRNA was one-tenth that in normal cells, but no differences were found in expression of other death-related molecules, including FasL (*11*). Bcl-xL protein was almost undetectable by immunoblot analysis of *RORγ*$^{-/-}$ thymocyte extracts (Fig. 2C). These results suggested that RORγ regulates DP thymocyte survival by enhancing expression of the anti-apoptotic molecule Bcl-xL.

The FSC profile of DP thymocytes from *RORγ*$^{-/-}$ mice (Fig. 1B) suggested that a malfunction of the cell cycle may accompany accelerated apoptosis. About 30% of thymocytes from *RORγ*$^{-/-}$ mice, but only 4 to 5% from heterozygous littermates, had greater than 2N DNA content, indicating that they were in the S/G_2 phases of the cell cycle (Fig. 3) (*12*). Thymocytes from *RORγ*$^{-/-}$ mice had reduced amounts of p27^{kip1}, which negatively regulates the transition from G_1 to S phase by inhibiting the activity of the cyclin-dependent kinase CDK2 (Fig. 2D). Correspondingly, CDK2 activity was increased 10-fold in mutant compared to wild-type cells (Fig. 2D) (*13*). When these thymocytes were cultured in the presence of the CDK inhibitor roscovitine, apoptosis was prevented, even though Bcl-xL expression was not restored (Fig. 2A) (*11*). Thus, CDK function is required for thymocyte apoptosis in the absence of RORγ, consistent with recent suggestions that anti-apoptotic Bcl-2 family members regulate CDK2 activity (*14, 15*).

Thymocytes with homozygous disruption of the *Bcl-xL* gene exhibit reduced survival similar to that in *RORγ*$^{-/-}$ mice (*16*). The thymic phenotype observed in *RORγ*$^{-/-}$ mice may thus be explained by the loss of positive regulation of Bcl-xL. To test this hypothesis, we prepared *RORγ*$^{-/-}$ mice that expressed *Bcl-xL* under the regulation of the *lck* gene proximal promoter, which directs expression in immature thymocytes (*17*). Bcl-xL expression in the *Bcl-xL*^{Tg}/*RORγ*$^{-/-}$ animals restored most aspects of normal thymocyte development (Fig. 3). Thymocyte number in *Bcl-xL*^{Tg}/*RORγ*$^{-/-}$animals was similar to that in *RORγ*$^{+}$ mice expressing the *Bcl-xL* transgene (about 1.5-fold higher than normal thymus) (Fig. 3B), and both DP and CD4 SP cells were present in normal numbers (Fig. 3C). TCR expression and the size of DP thymocytes were normal in the *Bcl-xL*^{Tg}/*RORγ*$^{-/-}$ mice, although the level of CD4 expression remained low (Fig. 3C). Both thymocyte survival and cell cycle regulation were corrected by the forced expression of Bcl-xL (Fig. 3, D and E). The latter was correlated with rescue of p27^{kip1} expression to wild-type levels (Fig. 3A). RORγ thus appears to act genetically upstream of Bcl-xL to prolong DP thymocyte survival and promote G_1 phase cell cycle arrest.

We crossed mice with a disrupted *TCR-Cα* gene, which does not express TCR on DP cells and, hence, cannot undergo negative selection, with *RORγ*$^{-/-}$ mice. *TCRα*$^{-/-}$/*RORγ*$^{-/-}$ thymocytes had the same phenotype as *RORγ*$^{-/-}$ thymocytes, indicating that negative selection signals do not initiate premature apoptosis in the absence of RORγ (*10*). This suggests that accelerated apoptosis is due to enhanced death by neglect. We also crossed RORγ-null mice to *gld/gld* mice, which are defective for FasL function (*18*). Thymocyte apoptosis in *gld/gld/RORγ*$^{-/-}$ mice was identical to that in *RORγ*$^{-/-}$ animals (*10*). Thus, the Fas:FasL system appears not to be regulated by RORγ to enhance thymocyte survival.

T cells in RORγ-deficient mice appeared to be exported normally to the periphery and to have normal proliferative functions (*11*). However, RORγ-deficient mice completely lacked lymph nodes and Peyer's patches (Fig. 4A) (*11, 19*). Development of lymph nodes and Peyer's patches is dependent on several tumor necrosis factor (TNF) family members (lymphotoxin α and lymphotoxin β, TRANCE/OPGL/RANKL) and their receptors (TNF receptor p55, lymphotoxin β receptor) (*20–25*). Mutations of these genes, with the exception of *TRANCE*, also result in disruption of splenic follicular structure and the absence of follicular dendritic cells. In contrast, splenic architecture and follicular dendritic cells were normal in *RORγ*$^{-/-}$ mice (*11*), suggesting that the membrane-bound form of lymphotoxin, LTαβ, and TNFα are produced normally in the follicles of mutant mice (*26*). Splenocytes from *RORγ*$^{-/-}$ mice contained one-third the normal number of T cells, but the proportion of CD4 and CD8 single-positive cells was unaffected (*11*). Lymphoid organ development was also defective in *gld/gld/RORγ*$^{-/-}$

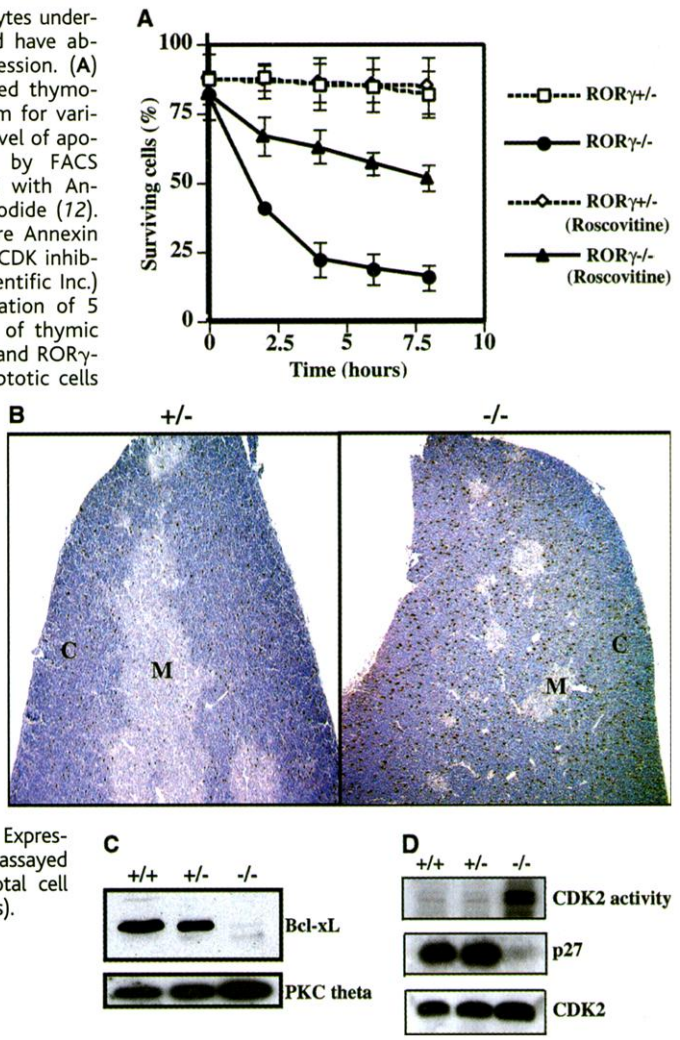

Fig. 2. *RORγ*$^{-/-}$ thymocytes undergo massive apoptosis and have abnormal cell cycle progression. (**A**) Survival of freshly isolated thymocytes, cultured in medium for various time intervals. The level of apoptosis was determined by FACS analysis of cells stained with Annexin V and propidium iodide (*12*). Percent of cells that were Annexin V^{-} PI^{-} is indicated. The CDK inhibitor roscovitine (A.G. Scientific Inc.) was used at a concentration of 5 μM. (**B**) TUNEL analysis of thymic sections from wild-type and RORγ-deficient mice (*12*). Apoptotic cells stain brown. C, cortex; M, medulla. (**C**) Immunoblot analysis of Bcl-xL levels in wild-type and mutant thymocytes. The blot was stripped and reprobed with antisera recognizing PKC-θ as a control for protein loading. (**D**) Reduced amount of p27^{kip1} and enhanced CDK2 activity in *RORγ*$^{-/-}$ thymocytes. CDK2 was immunoprecipitated and subjected to in vitro kinase assay using Histone H1 as substrate (*13*) (top panel). Expression of p27 and CDK2 was assayed by immunoblotting of total cell extracts (lower two panels).

mice, indicating that this phenotype is unrelated to loss of repression of FasL expression.

The absence in mutant mice of lymph nodes and Peyer's patches despite normal splenic B cell follicle development suggested that, although LTαβ and TNFα can be produced by splenic B cells, there may be a defect in other cells that produce these cytokines. When *RORγ*$^{-/-}$ fetal liver stem cells were transferred into *RAG2*$^{-/-}$ mice, normal reconstitution of all secondary lymphoid organs of the recipient mice occurred, indicating that defective lymph node development in *RORγ*$^{-/-}$ animals cannot be attributed to defects in T or B cell homing (*11*). We analyzed cells with the cell-surface phenotype CD3$^-$CD4$^+$CD45$^+$IL-7Rα$^+$, which are associated with early lymph nodes in fetal mesentery, produce lymphotoxin (*19*), and may function in lymphoid organ development (*27*). These cells express large amounts of RORγ mRNA (*10*). CD3$^-$CD4$^+$CD45$^+$ cells were absent from both mesentery and intestines of E16.5 and E18.5 mutant embryos and of 2-day-old mutant mice (Fig. 4B) (*11*). In normal embryos, expression of RORγ was detected in cell clusters flanking the pharynx, intestines, and pericardium as early as E12.5 (Fig. 4, C and D) (*10, 28*). Many of the cells that expressed nuclear RORγ also expressed cell-surface CD4 (Fig. 4E). In E14.5 embryos, near the limb buds we observed bilateral clusters of cells expressing RORγ, where axillary and inguinal lymph nodes develop (*11*). These results suggest that RORγ is required for the development of CD4$^+$ progenitor cells involved in the morphogenesis of lymph nodes and Peyer's patches.

Our results indicate that RORγ is essential for survival of immature CD4$^+$CD8$^+$ thymocytes and for development of lymphoid organs. The defect in thymocyte development in mice lacking RORγ can be attributed directly to its regulation of Bcl-xL expression in DP thymocytes. Anti-apoptotic effects of Bcl-xL provide these cells the opportunity to interact with MHC/peptide complexes and undergo positive selection. Regulated shut-off of RORγ expression, or ligand-mediated regulation of RORγ function, could attenuate Bcl-xL expression and result in thymocyte death by neglect. Bcl-xL also promotes maintenance of high p27^{kip1} levels; in its absence, the increased CDK2 activity contributes to cell death. Thymocytes lacking Bcl-xL display accelerated apoptosis, similar to that observed in the *RORγ*-null animals, but it is not known whether they also have a defect in cell cycle progression (*16*).

Disruption of the gene encoding the transcriptional repressor Id2 results in a lymphoid organ phenotype similar to that of *RORγ*$^{-/-}$ mice (*29*). Interestingly, both Id2 and RORγ transcripts were detected in CD3$^-$CD4$^+$CD45$^+$IL-7Rα$^+$ cells (*10, 29*), and this cell population was undetectable in animals lacking either Id2 or RORγ (Fig. 4B) (*29*). Thus, Id2 and RORγ may both be required for survival or differentiation of these hematopoietic progenitors, which may be essential at an early stage of lymphoid organ development.

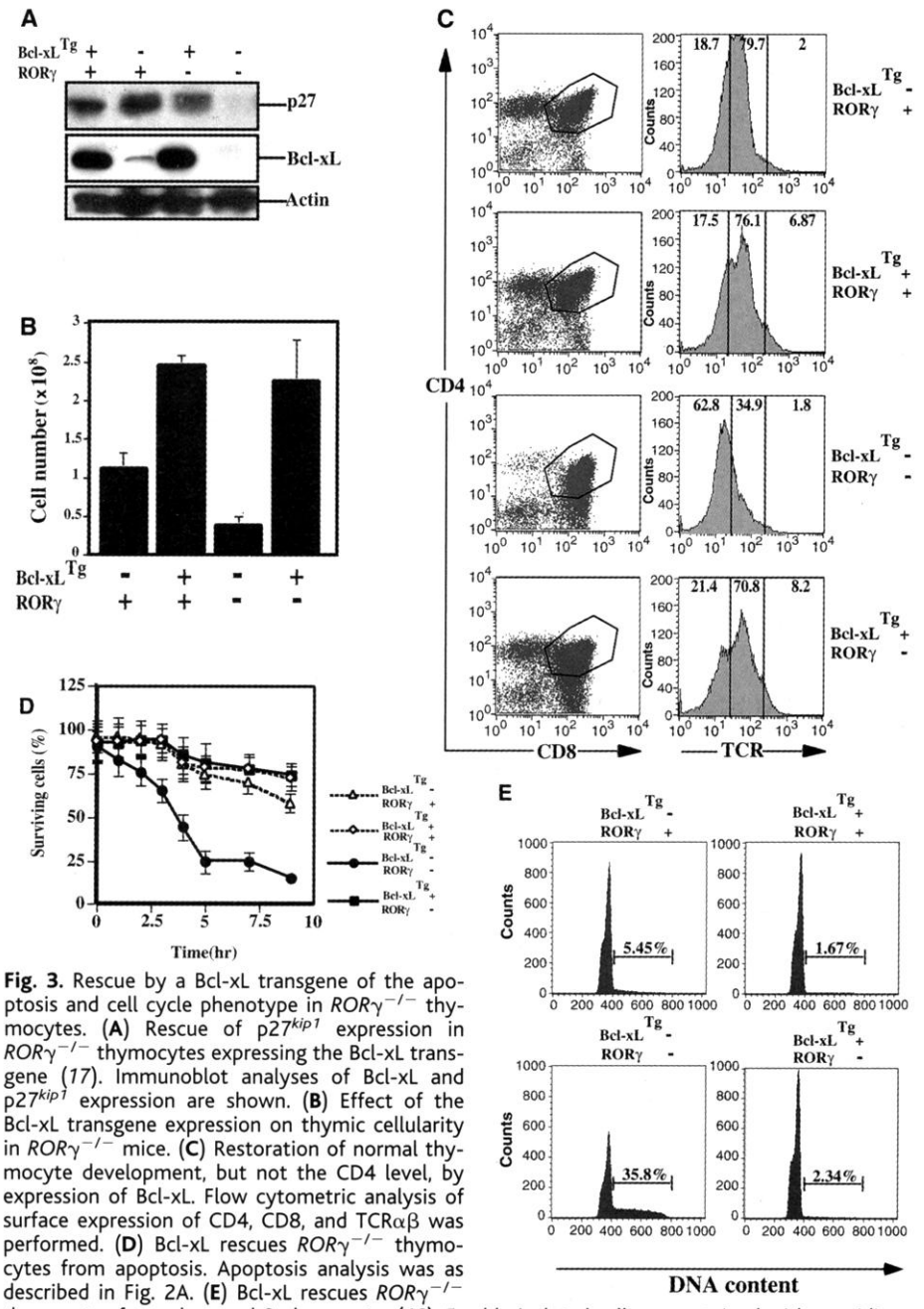

Fig. 3. Rescue by a Bcl-xL transgene of the apoptosis and cell cycle phenotype in *RORγ*$^{-/-}$ thymocytes. (**A**) Rescue of p27^{kip1} expression in *RORγ*$^{-/-}$ thymocytes expressing the Bcl-xL transgene (*17*). Immunoblot analyses of Bcl-xL and p27^{kip1} expression are shown. (**B**) Effect of the Bcl-xL transgene expression on thymic cellularity in *RORγ*$^{-/-}$ mice. (**C**) Restoration of normal thymocyte development, but not the CD4 level, by expression of Bcl-xL. Flow cytometric analysis of surface expression of CD4, CD8, and TCRαβ was performed. (**D**) Bcl-xL rescues *RORγ*$^{-/-}$ thymocytes from apoptosis. Apoptosis analysis was as described in Fig. 2A. (**E**) Bcl-xL rescues *RORγ*$^{-/-}$ thymocytes from abnormal S-phase entry (*12*). Freshly isolated cells were stained with propidium iodide, and flow cytometric analysis was performed to detect DNA content in each cell. The bracketed regions demark cells possessing >2N amounts of DNA.

References and Notes

1. A. W. Goldrath and M. J. Bevan, *Nature* **402**, 255 (1999).
2. C. D. Surh and J. Sprent, *Nature* **372**, 100 (1994).
3. L. B. King *et al.*, *Immunity* **3**, 647 (1995).
4. B. J. Calnan, S. Szychowski, F. K. Chan, D. Cado, A. Winoto, *Immunity* **3**, 273 (1995).
5. T. Hirose, R. J. Smith, A. M. Jetten, *Biochem. Biophys. Res. Commun.* **205**, 1976 (1994).
6. M. A. Ortiz, F. J. Piedrafita, M. Pfahl, R. Maki, *Mol. Endocrinol.* **9**, 1679 (1995).
7. Y. W. He, M. L. Deftos, E. W. Ojala, M. J. Bevan, *Immunity* **9**, 797 (1998).
8. D. R. Littman *et al.*, *Cold Spring Harbor Symp. Quant. Biol.* **64**, 373 (1999).
9. The targeting vector for the inactivation of the RORγ gene was constructed using the PL2-Neo vector by replacing the exon encoding the DNA-binding domain of RORγ with the *neomycin* resistance gene. Three of 150 G418-resistant E14 ES cell clones were positive for homologous recombination. Two of these were used to generate chimeric founder mice by microinjection into C57BL/6J blastocysts (*10*).

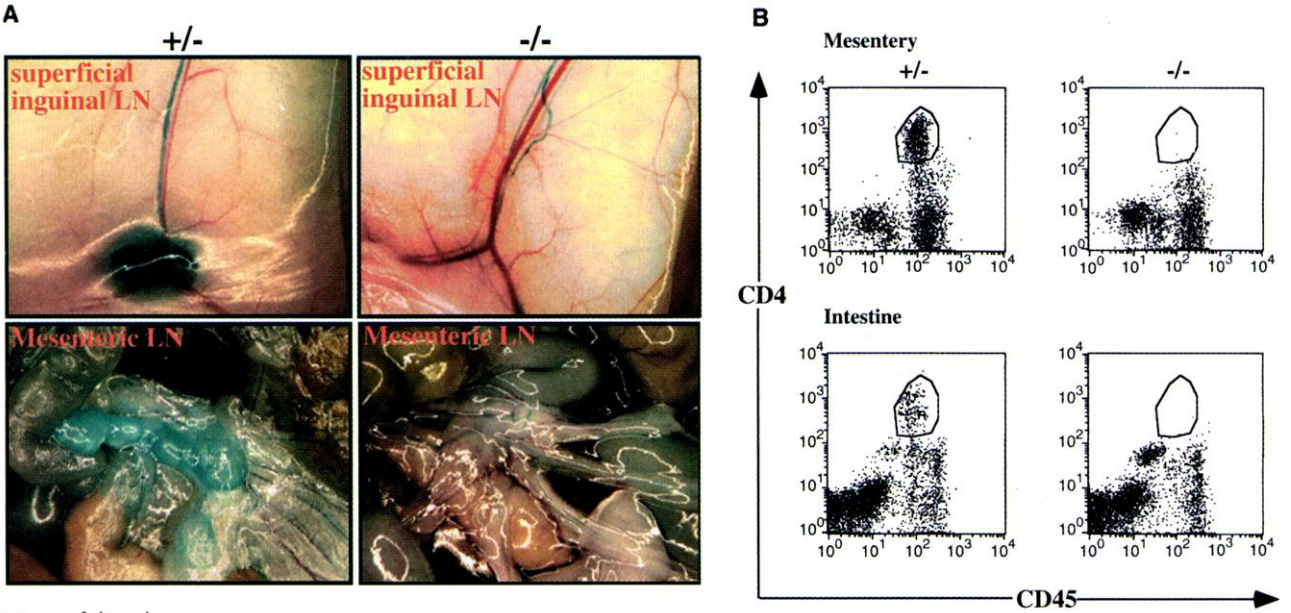

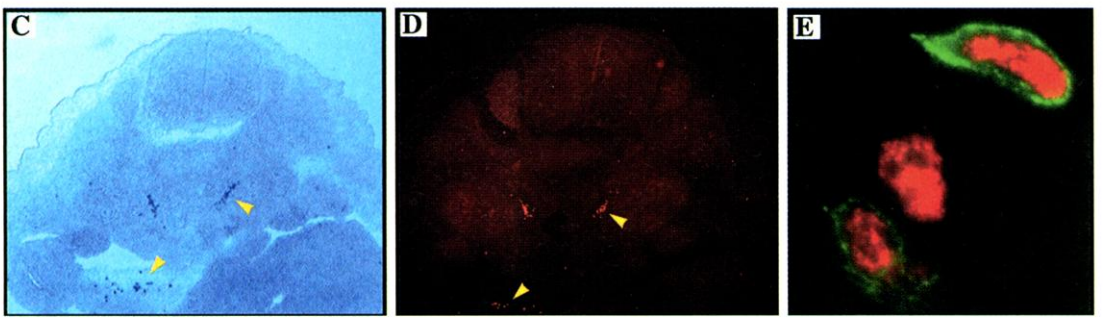

Fig. 4. Absence of lymph node development and of $CD3^{-}CD4^{+}CD45^{+}$ putative lymphoid organ precursors in *ROR*$\gamma^{-/-}$ mice. (**A**) Lymph nodes were visualized by Evan's blue dye, which identifies both superficial inguinal and mesenteric lymph nodes (*19*). (**B**) Loss of $CD3^{-}CD4^{+}CD45^{+}$ cells from mesentery and intestines of E18.5 mutant animals. Flow cytometry was used to analyze live cells for expression of CD4 and CD45 (*19*). Gated $CD4^{+}CD45^{+}$ cells lacked expression of CD3. (**C** through **E**) Expression pattern of RORγ in E12.5 mouse embryos (*10*). (C) Detection of RORγ mRNA by in situ hybridization of transverse section. Arrows mark expression in regions flanking the esophagus and a region dorsal to the fetal liver. (D) Expression of RORγ protein in a section serial to that shown in (C). (E) Expression of CD4 (green) in some, but not all, RORγ-expressing cells (red). Magnification: (C and D): ×5; (E): ×63.

10. Supplemental material is available at www.sciencemag.org/feature/data/1048806.shl
11. Z. Sun *et al.*, unpublished data.
12. Thymocytes (2×10^5) were washed twice with phosphate buffered saline (PBS) and incubated with FITC-conjugated Annexin V (Pharmingen) and 200 ng/ml propidium iodide (PI) for 15 min on ice in Annexin V binding buffer (0.01 M Hepes, pH 7.4; 0.14 mM NaCl; 2.5 mM $CaCl_2$). Two hundred microliters of binding buffer were added to the above staining sample. Dead cells were detected by flow cytometry analysis as Annexin V– and PI-positive cells. For in situ TUNEL analysis, freshly isolated thymi were fixed overnight in 63% ethanol, 5% acetic acid, and 1.8% formaldehyde. The fixed tissues were paraffin-embedded and sectioned. Apoptotic cells were detected with a TUNEL analysis kit (Intergen) according to the manufacturer's protocol. For cell cycle analysis, freshly isolated thymocytes (10^6 cells) were washed twice with PBS and then resuspended in 300 μl of PBS. Cold ethanol (700 μl) was slowly added to the resuspended cells while vortexing. The cells were incubated on ice for 1 hour and washed twice with PBS. Fixed cells were resuspended in 1 ml of staining buffer (1× PBS, 0.1% NP-40, 0.1 mg/ml RNase A, and 0.05 mg/ml PI) and incubated on ice for 20 min. DNA content of cells was analyzed using flow cytometry.
13. CDK2 was immunoprecipitated from 2×10^7 thymocytes lysed in 50 mM tris, pH 7.4, 50 mM NaCl, 0.5% NP-40 in the presence of proteinase inhibitors (Boehringer Mannheim). Immune complexes were washed twice with lysis buffer and twice with kinase buffer (20 mM tris, pH 7.4, 10 mM $MgCl_2$ and 1 mM DTT). Subsequently immune complexes were incubated with 50 μl of kinase buffer containing 2 μg of Histone H1, 10 μCi of [γ-^{32}P]ATP at 30°C for 30 min. The reaction was terminated by heat inactivation at 100°C for 5 min. The reaction mixture was resolved on a 12% SDS-PAGE gel which was then dried and autoradiographed for 4 hours.
14. S. Mazel, D. Burtrum, H. T. Petrie, *J. Exp. Med.* **183**, 2219 (1996).
15. G. Gil-Gomez, A. Berns, H. J. Brady, *EMBO J.* **17**, 7209 (1998).
16. A. Ma *et al.*, *Proc. Natl. Acad. Sci. U.S.A.* **92**, 4763 (1995).
17. D. T. Chao *et al.*, *J. Exp. Med.* **182**, 821 (1995).
18. T. Takahashi *et al.*, *Cell* **76**, 969 (1994).
19. For visualization of lymph nodes, 250 μl of 1% Evans blue dye (Sigma) was injected into the hind footpads of mice. After 30 min, mice were sacrificed and superficial inguinal lymph nodes were visualized and documented under a dissecting microscope using a digital camera. For mesenteric lymph node visualization, mice were sacrificed 1 to 1.5 hours after injection of Evans blue dye. For analysis of precursors, the mesentery of each embryo was dissected away from the intestines and both were digested separately using collagenase type IV (Sigma) [0.5 mg/ml in PBS containing 2% fetal bovine serum (FBS)] for 30 min. The cells were washed and subsequently stained with CD45-FITC, CD4-PE, and CD3-biotin (Pharmingen), washed, and incubated with Streptavidin-CyChrome (Pharmingen). After washing, the cells were resuspended in PBS containing 2% FBS and 7-AAD, to discriminate live versus dead cells.
20. P. De Togni *et al.*, *Science* **264**, 703 (1994).
21. M. B. Alimzhanov *et al.*, *Proc. Natl. Acad. Sci. U.S.A.* **94**, 9302 (1997).
22. P. A. Koni *et al.*, *Immunity* **6**, 491 (1997).
23. Y. Y. Kong *et al.*, *Nature* **397**, 315 (1999).
24. B. Neumann, A. Luz, K. Pfeffer, B. Holzmann, *J. Exp. Med.* **184**, 259 (1996).
25. A. Futterer, K. Mink, A. Luz, M. H. Kosco-Vilbois, K. Pfeffer, *Immunity* **9**, 59 (1998).
26. R. Endres *et al.*, *J. Exp. Med.* **189**, 159 (1999).
27. R. E. Mebius, P. Rennert, I. L. Weissman, *Immunity* **7**, 493 (1997).
28. E12.5 mouse embryos were dissected and fixed in 4% paraformaldehyde, 0.1 M phosphate buffer (PB) (pH 7.4) at 4°C for 1 to 2 hours, washed with PBS, equilibrated with 30% sucrose, 0.1 M PB, and mounted in OCT embedding medium. Frozen 11 μM cryostat sections were mounted on SuperFrost Plus slides (Fisher) and subsequently analyzed by in situ hybridization or immunohistochemistry (*10*). Antibodies used were hamster monoclonal anti-RORγ (diluted 1:10) and Alexa-488-conjugated anti-CD4 (diluted 1:200). Cy3-conjugated goat anti-hamster (Jackson Immuno Research Laboratory) was used at 1:700 dilution. Images were collected on a Zeiss Axioplan 2 microscope using Slidebook software (Innovative Imaging). A digoxigenin-labeled antisense riboprobe complementary to the RORγ cDNA was synthesized according to supplier protocol (Boehringer Mannheim). The hamster monoclonal antibody against murine RORγ was prepared using a His-tagged RORγ expressed in bacteria as immunogen (*10*).
29. Y. Yokota *et al.*, *Nature* **397**, 702 (1999).

30. We thank F. Weis-Garcia for preparation of mAbs, S. Jung and R. Lang for help with microscopy, S. Smith for the TUNEL analysis, J. McMicking for assistance with intestinal lymphoid organ analysis, S. Korsmeyer for Bcl-xL transgenic mice, P. Rennert and H. Petrie for helpful discussions, and Y. Choi, W. Ellmeier, and L. Johnston for comments on the manuscript. Supported by an NIH Molecular Oncology and Immunology training grant (Z.S.), the Royal Netherlands Academy of Arts and Sciences (R.E.M.), a postdoctoral fellowship from the Irvington Institute (Y.-R.Z.), and the Howard Hughes Medical Institute (D.R.L.).

20 January 2000; accepted 4 May 2000

A Subset of Viral Transcripts Packaged Within Human Cytomegalovirus Particles

Wade A. Bresnahan and Thomas Shenk*

A human cytomegalovirus gene array was used to identify a previously unidentified class of viral transcripts. These transcripts, termed virion RNAs, were packaged within infectious virions and were delivered to the host cell on infection. This mechanism of herpesvirus gene expression allows for viral genes to be expressed within an infected cell immediately after virus entry and in the absence of transcription from the viral genome.

Human cytomegalovirus (HCMV), like all herpesviruses, regulates its gene expression in a coordinated cascade (*1*). HCMV genes are classified as immediate early, early, or late, depending on their kinetics of expression and the conditions under which they are transcribed. Regardless of the class of the gene, it has been assumed that all HCMV RNAs present in the infected cell are transcribed from the DNA genome of the infecting virus. Recently, it was noted that RNA copurified with virions (*2*). Using gene array technology, we identified a subset of HCMV transcripts that were packaged within HCMV virus particles and delivered to the host cell upon infection. Delivery of virion RNAs to the host cell allows for their expression immediately after virus entry in the absence of new transcription.

Specific RNAs in virus particles were screened for with an HCMV gene array. The array of polymerase chain reaction (PCR)–amplified fragments includes DNAs corresponding to all 208 open reading frames (ORFs) in the HCMV AD169 genome (*3*, *4*), making it possible to assay most HCMV transcripts in a single experiment. Initially, the arrays were validated by hybridization to radioactive probes prepared by random priming of cosmids, whose inserts collectively included about 90% of the HCMV genome (Fig. 1A). The amount of probe hybridizing to each spot on the array was about the same, confirming that the spots contained similar amounts of target DNA, and the hybridization of each probe was restricted to its cognate set of target DNAs, verifying the specificity of the assay.

To probe the identity of RNA that copurified with virions, we generated radioactively labeled cDNA by reverse transcription of RNA isolated from virus particles and used it to probe the HCMV gene array (*5*). HCMV RNAs corresponding to ORFs UL21.5, UL106-109, TRL/IRL 2-5, TRL/IRL 7, and TRL/IRL 13 were detected (Fig. 1B). UL21.5, originally termed R28070 (*6*), is a late mRNA (*6*, *7*), UL106-109 corresponds to a 5-kb immediate early RNA (*8*), TRL/IRL 2-5 is a 2.7-kb early RNA (*9*, *10*), and TRL/IRL 7 is a 1.2-kb early RNA (*9*, *10*). Analysis of RNA from infected cells confirmed the sizes and accumulation patterns of these RNAs (Fig. 2A, lanes 1 to 4). All of the RNAs accumulated to maximal levels late after infection, when virions are being assembled. The functions of the proteins encoded by these RNAs are unknown.

To confirm the results obtained with the HCMV gene array and to verify that RNA was detected rather than contaminating DNA, we performed a Northern blot assay on RNA from virus particles. Particles were purified and treated with ribonuclease one (RNase One), and deoxyribonuclease I (DNase I)–treated RNA was isolated. Equal portions of virion RNA were either mock-treated or treated with RNase One and then analyzed by Northern blot assay with probes for the RNAs identified in Fig. 1B. The samples were sensitive to RNase One (Fig. 2A, lanes 6 and 7), and the virion RNAs migrated identically to polyadenylated RNAs isolated from infected cells (Fig. 2A, lanes 6 and 8). These observations, together with the fact that the probes were made by reverse transcription with an

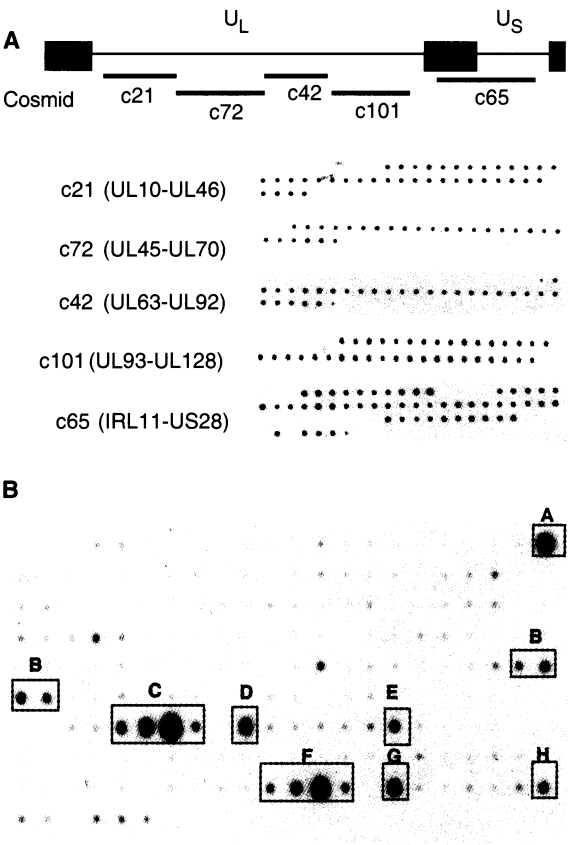

Fig. 1. Characterization of an HCMV DNA array and identification of HCMV transcripts packaged within virus particles. **(A)** HCMV gene arrays (*3*) were probed with individual [^{32}P]-labeled cosmids to confirm specificity of the ORFs spotted on the arrays. **(B)** An HCMV gene array was probed with [^{32}P]-labeled cDNA generated by reverse transcription of DNase I–treated RNA isolated from HCMV particles. The transcripts identified correspond to the predicted ORFs UL21.5 (A), UL106-109 (B), IRL/TRL 2-5 (C and F), IRL/TRL 4 (D and G), and IRL/TRL13 (E and H). Lighter spots observed in the array that are not marked by boxes were not consistently positive in repeated experiments.

Department of Molecular Biology, Princeton University, Princeton, NJ 08544, USA.

*To whom correspondence should be addressed. E-mail: tshenk@princeton.edu